Spiral Waves in Two-Dimensional Models of Ventricular Muscle: Formation of a Stationary Core

Jacques Beaumont, Nicolas Davidenko, Jorge M. Davidenko, and José Jalife
Department of Pharmacology, SUNY Health Science Center at Syracuse, Syracuse, New York 13210 USA

ABSTRACT Previous experimental studies have clearly demonstrated the existence of drifting and stationary electrical spiral waves in cardiac muscle and their involvement in cardiac arrhythmias. Here we present results of a study of reentrant excitation in computer simulations based on a membrane model of the ventricular cell. We have explored in detail the parameter space of the model, using tools derived from previous numerical studies in excitation-dynamics models. We have found appropriate parametric conditions for sustained stable spiral wave dynamics (1 s of activity or ~10 rotations) in simulations of an anisotropic (ratio in velocity 4:1) cardiac sheet of 2 cm × 2 cm. Initially, we used a model that reproduced well the characteristics of planar electrical waves exhibited by thin sheets of sheep ventricular epicardial muscle during rapid pacing at a cycle length of 300 ms. Under these conditions, the refractory period was 147 ms; the action potential duration (APD) was 120 ms; the propagation velocity along fibers was 33 cm/s; and the wavelength along fibers was 4.85 cm. Using cross-field stimulation in this model, we obtained a stable self-sustaining spiral wave rotating around an unexcited core of 1.75 mm × 7 mm at a period of 115 ms, which reproduced well the experimental results. Thus the data demonstrate that stable spiral wave activity can occur in small cardiac sheets whose wavelength during planar wave excitation in the longitudinal direction is larger than the size of the sheet. Analysis of the mechanism of this observation demonstrates that, during rotating activity, the core exerts a strong electrotonic influence that effectively abbreviates APD (and thus wavelength) in its immediate surroundings and is responsible for the stabilization and perpetuation of the activity. We conclude that appropriate adjustments in the kinetics of the activation front (i.e., threshold for activation and upstroke velocity of the initiating beat) of currently available models of the cardiac cell allow accurate reproduction of experimentally observed self-sustaining spiral wave activity. As such, the results set the stage for an understanding of functional reentry in terms of ionic mechanisms.

INTRODUCTION

Electrical wave propagation in the heart shares many of the properties of wave propagation in other excitable media (Winfree, 1986). One such property is the ability to undergo vortex-like reentry (Davidenko et al., 1991a; Pertsov et al., 1993), which has also been demonstrated in other biological systems, such as the brain and retina (Gorelova and Bures, 1983), the social amoeba *Dyctiostelium* (Gerish, 1965), and calcium waves in *Xenopus laevis* oocytes and single ventricular myocytes (Lechleiter et al., 1991), as well as in autocatalytic chemical reactions (Winfree, 1972). In all such systems, a particular perturbation of the excitation wave may result in vortex-like activity. In general, during such activity the excitation wave acquires the shape of a spiral (Krinsky, 1978), which rotates around an organizing center or core and is called a *spiral wave*.

Spiral waves have been extensively studied in chemical media (Winfree, 1972), as well as in the FitzHugh-Nagumo model (Pertsov et al., 1984; Winfree, 1991; Starobin et al., 1996), and recent studies have provided evidence favoring the applicability of spiral wave theory to the understanding of vortex-like reentry in the heart (see Gray et al., 1995, for a brief review). However, there remain many intriguing questions that relate to the underlying mechanisms of this activity, particularly in relation to the ionic basis of the formation of the core and stabilization of the activity. More specifically, Davidenko et al. (1990, 1991a,b) and Pertsov et al. (1993) clearly demonstrated that thin square slices of sheep ventricular epicardial muscle of ~2 cm × ~2 cm could undergo self-sustained reentrant excitation for long intervals of time (sometimes longer than 20 min) at stable periods of rotation that ranged between 117 and 250 ms (see Table 2). Most importantly, the activity occurred in preparations whose wavelength (i.e., space occupied by the excited state) during plane wave propagation in the longitudinal direction of the cardiac fibers was about three times larger than the size of the preparation. This observation is particularly intriguing and may have importance in discerning the mechanisms of maintenance of reentrant cardiac arrhythmias. Its understanding is, in fact, the main focus of this study.

Previous simulation studies (Courtemanche, 1996; Courtemanche and Winfree, 1991; Leon et al., 1994; Efimov et al., 1995) using the model developed by Beeler and Reuter (BR model; 1977) have shown that sustained vortex-like activity in a small two-dimensional matrix of cells requires that the model be modified by reducing its action potential duration (APD) or its velocity of propagation. For example, in the study of Efimov et al. (1995), the velocity was

Received for publication 17 January 1997 and in final form 26 March 1998.

Address reprint requests to Dr. Jacques Beaumont, Department of Pharmacology, SUNY Health Science Center at Syracuse, 766 Irving Ave., Syracuse, NY 13210. Tel.: 315-464-5138; Fax: 315-464-8000; E-mail: beaumont@sunrise.pharm.hscsyr.edu.

0006-3495/98/07/01/14 $2.00

reduced by decreasing G_{Na}. On the other hand, Leon et al. (1994) observed stable and regular vortex-like activity only if the APD was reduced to 45 ms. In the latter case, the rotation period was 60 ms. Although the above simulation results addressed part of the wide spectrum of the behavior of vortex-like reentry in cardiac muscle, they departed significantly from the experimental results obtained in isolated preparations (Davidenko et al., 1990, 1991a,b; Pertsov et al., 1993). Here we start from the premise that well-targeted modifications of an existing membrane model may allow simulation of experimental results, as well as accurate predictions regarding spiral wave dynamics and mechanisms. We base such a premise on results obtained previously in other excitable media. These include the following. First, an extensive study of the FitzHugh-Nagumo model (Winfree, 1991) during spiral wave activity has demonstrated regions in parameter space where the size of a circular core can be accurately controlled. Second, it has been shown (Efimov et al., 1995) that spiral waves in the BR model exhibit behavioral characteristics that are similar to those observed with the FitzHugh-Nagumo model, e.g., flower-like meandering patterns (epicycloidal, cycloidal, hypocycloidal), circular (or elliptical) linear cores, and an excitable gap between repetitive spiral wave rotations, all of which constitute generic behavior of all excitable media (Krinsky and Efimov, 1992; Winfree, 1991, Efimov et al., 1995). Inspired by these results, we have used the Luo and Rudy model (1991) and modifications thereof to extend previous explorations of the parameter space of existing ionic models (Efimov et al., 1995; Courtemanche, 1996; Courtemanche and Winfree, 1991; Leon et al., 1994) and search for regions where the core size and excitable gap can be accurately controlled.

This paper is organized as follows. First, in Materials and Methods we introduce the ionic model used in the study and provide some useful definitions, as well as the technical details of the simulations. Then in the Results, the section Predictions of Existing Model illustrates how existing model predictions depart from experimental results. Subsequently, in the section titled Role of the Kinetics of the Activation Front, we provide arguments for the need of an appropriate definition of the kinetics of the activation front to make better model predictions. We test this postulate in the subsequent section, Exploring the Parameter Space of the SAPD Model, by examining spiral wave behavior when varying three parameters that control different aspects of the kinetics of the activation front. This exploration of the parameter space was performed using a model that exhibited a very small action potential duration (SAPD model). This was purposely done with the idea of generating sustained spiral wave activity in a small spatial domain. The exercise showed that small changes in the appropriate direction of the parameter space can dramatically alter the behavior and, in fact, result in a relatively large core and a large excitable gap. Finally, in the section Stationary Spiral Wave Activity in an Anisotropic Membrane Model, we show that accurate reproduction of experimentally observed spiral wave activity is possible once appropriate kinetics of the activation front are incorporated into a more realistic action potential model. Under such conditions, we were able to induce stationary spiral wave activity by using a model whose refractory period during planar wave propagation (up to 235 ms) was about twice as large as the cycle length of the spiral. In the Discussion we present the limitations of the model introduced in this study and the implications of our findings for the understanding of life-threatening arrhythmias.

MATERIALS AND METHODS

Model

We used a continuous ionic model to study the propagation of electrical impulses in the heart muscle. In this formulation, membrane channels are distributed uniformly at the surface of a cardiac sheet. Changes in the conductance of the membrane channels are governed by Hodgkin-Huxley-type equations (Hodgkin and Huxley, 1952). The partial differential equation governing the propagation is obtained by applying the law of conservation of charge in a small unit volume. The resulting equations are as follows:

$$-C_p \frac{\partial V}{\partial t} + \upsilon \nabla \cdot D \nabla V = \sum_s I_{ion_s}(V, t) + I_0(x, t) \qquad (1)$$

$$I_{ion_s}(V, t) = \begin{cases} G_s(V)(V - E_s) \\ \quad \text{if nongated current} \\ G_s(V)\left(\prod_{k=0}^{k=K(s)} (y_{k,s}(V, t))^{\lambda_{k,s}}\right)(V - E_s) \\ \quad \text{if gated current} \end{cases} \qquad (2)$$

$$\frac{dy_{k,s}(V, t)}{dt} = \frac{(Y_{k,s}(V - \psi_{k,s}) - y_{k,s}(V, t))}{\tau_{k,s}(V) + \epsilon_{k,s}} \qquad (3)$$

Definition

The meaning of each of the variables and parameters used is given in Table 1. Our model incorporates seven ionic currents. The conductance of each current, as well as the steady state and time constant for each gating variable, are given in the paper by Luo and Rudy (1991). Below in the text, we use the subscripts Na and K for the sodium and potassium currents, respectively. Similarly, the sodium current has three molecular gates (or gating variables), and we refer to them using the subscripts m, h, and j (e.g., τ_m for the time constant of the m-gate of the sodium current and ϵ_m for an offset to this time constant). By activation and inactivation gates we mean gates that open or close (0 is closed, 1 is open) upon depolarization. In the above formulation, the m-gate is an activation gate, whereas the h-gate and j-gate are inactivation gates. In all simulations, we used no-flux boundary conditions on the border of the rectangular domain. The function $I_o(x, t)$ of the source term of Eqs. 1–3 was used to apply the current stimulus.

The term spiral *wave activity* is used here as a synonym of *vortex-like* or *functional* reentry, i.e., reentrant activity in the absence of an anatomical obstacle. The spiral revolves around an organizing center or *core*, which may be stationary or may drift, depending on the characteristics of the medium. The *excitable gap* is the interval of time during which the tissue remains excitable. The existence of an excitable gap indicates that a large portion of the rotating activation front evolves in fully recovered areas, which is presumed to be important for the stationarity of the motion.

Numerical methods

The system of equations was solved using a finite-element method (FEM) and a semiimplicit integration scheme (Beaumont et al., 1995a). In numer-

TABLE 1 Variables and parameters of the model

Variable	Definition	Unit
x*	Vector (two components) representing the distance along the orthogonal axes of the system x_0 longitudinal, x_1 transverse	cm
t	Time	ms
$V(x, t)$	Membrane potential	mV
C_p	Capacitance of the membrane $C_p = 1$ for cardiac cells	$\mu F/cm^2$
v	Volume-to-surface ratio of the cell membrane	cm
ρ_L, ρ_T	Axial resistivity along the longitudinal (L) and transverse (T) directions with respect to fiber orientation	$K\Omega$ − cm
D	Tensor of diffusion, 2 × 2 diagonal matrix with coefficients $1/\rho_L$ and $1/\rho_T$	$1/K\Omega$ − cm
$I_{ion_s}(V, t)$	Ionic current of a species s	$\mu A/cm^2$
$I_0(x, t)$	Current stimulus	$\mu A/cm^2$
$G_s(V)$	Maximum conductance of a channel of an ion species s	mS
E_s	Reversal potential of an ionic current s	mV
$y_{k,s}(V, t)^{\#}$	Fraction of a population of a gate k of a channel (or ionic current) s in the open state	No unit
$Y_{k,s}(V)^{\#}$	Steady state of the gating variable $y_{k,s}$	No unit
$\psi_{k,s}$	Voltage shift of the steady state characteristics of the gating mechanism	mV
$K(s)$	Number of different molecular gates in a channel or in a gated current s	No unit
$\lambda_{k,s}^{\#}$	For a given gate (k, s), number of similar particles that should be simultaneously in the open state to open a channel	No unit
$\tau_{k,s}(V)^{\#}$	Time constant of a gate k related to a channel (or current) s	ms
$\epsilon_{k,s}^{\#}$	Constant offset added to a given time constant	ms

*The longitudinal axis is horizontal in all displays.
#In the text the indices k, s are sometimes replaced by a letter, e.g., Na and K stand for sodium and potassium currents; m, h, and j stand for the activation and inactivation gates (there are two) of the sodium current.

ical calculations we used interpolation polynomials of degree 3, an error tolerance of 0.01 mV, and a time step of 100 μs. The integration procedure used implicitly an approximation of the solution at $t + dt$. This approximation was iteratively refined at each time step. The iteration process stopped when the difference between two successive approximations was not larger than the tolerance. The mesh size was adjusted to have a phase shift of less than 0.1 ms after 60 ms of integration (60 cubic elements for a cable, 2 cm long, with an axial resistivity of 200 Ω-cm). Four nodes per element were used (16 nodes in 2D), which implied an internode spacing of 111 μm (nodes at the border of an element are shared). Previously, we presented convergence tests of the numerical method used in this study (Beaumont et al., 1995a). The results demonstrated that the error was well controlled. Finally, the analysis of our simulation results required measurements of wave front curvature along isopotentials. Details of the numerical calculations are provided in the Appendix.

Most simulations were performed on the supercomputer (IBM SP) at the Cornell Theory Center of Cornell University. The software ran in parallel on 12 processors. The parallel version of our code was constructed using the message-passing interface library of IBM (MPIF). To facilitate comparison with experimental results, simulation results were animated on the computer with AVS (Advanced Visual Systems) software.

RESULTS

Predictions of existing membrane models: the LR model

We used the 1991 version of the Luo and Rudy model (LRI model; Luo and Rudy, 1991). As done previously by others (Leon et al., 1994), we have fixed the reversal potential of the slow inward current (E_{si} set to 80 mV), which is appropriate because, although Reuter and Scholz (1977) observed that E_{si} is sensitive to changes in the external concentration of calcium, they did not observe significant changes in E_{si} when voltage clamping the membrane of cardiac cells. To simulate experimental results obtained in thin sheets of ventricular epicardial muscle, we used a square sheet (2 cm × 2 cm) of membrane model cells in which the channels were uniformly distributed. We chose a continuous model because previous modeling (Buchanan et al., 1990) and experimental studies (Fast and Kleber, 1993, 1994; Fast et al., 1996) suggested that it was a good representation of the ventricular tissue. We used an axial resistivity of 200 Ω-cm, a volume-to-surface ratio of 2.5 μm, and a capacitance of 1 μF/cm^2, all of which represent physiological conditions (Kleber and Riegger, 1987; Weidman, 1970; Daut, 1982).

Spiral waves were initiated using cross-field stimulation (Pertsov et al., 1993). In our model, electrical stimulation was applied by injecting current across the membrane on a given area ($I_o(x, t)$; see Eq. 1). We refer to this area as a "stimulating electrode." A stimulating electrode (E1) of 2 mm × 2 cm was placed vertically on the left side of the array. A second electrode (E2) was placed on the lower left quadrant. The size of E2 was 1 cm × 0.8 cm. A planar wave (S1) was initiated by electrode E1. When the tail of S1 produced a gradient of refractory state in the preparation, a second wave (S2) was initiated at E2. If timing was appropriate, S2 produced a spiral wave. The stimulus amplitudes were 1.5 and 3 times threshold for S1 and S2, respectively; in both cases, the stimulus duration was 5 ms. Only in the case of the LRI model was it necessary to deliver a third hyperpolarizing stimulus (S3) at electrode E2 (−9 μA/cm^2, for 5-ms duration, 20 ms after stimulus S2) to initiate reentry.

Usually the area under E2 remained depolarized for a long period of time (~100 ms) after the application of S2, which prolonged local refractoriness and interfered with the rotating spiral. S3 induced repolarization and enabled spiral

wave initiation in this model. Yet we were unable to obtain sustained spiral wave activity when using the original LRI model. The sequence of frames shown in Fig. 1 A illustrates the evolution in space and time of the excitation pattern, 60 to 130 ms after cross-field stimulation. Between 90 and 130 ms, the wave front came closer and closer to the wave tail, until it was unable to propagate and the activity terminated (not shown).

The above results are not surprising. Without any modifications, the LR model exhibits a wavelength of 28 cm (see Table 3). Therefore in a 2 cm × 2 cm preparation, it seems impossible to have enough recovery ahead of an activation front to allow for the stability of a reentrant wave. We cannot exclude the possibility that simulations using a more realistic model of the current distribution during application of the triggering stimulus may lead to different predictions. However, a recent study of spiral wave activity using the BR model and a bidomain formulation (Roth, 1997) strongly suggests that it would not change this conclusion. Most importantly, according to current knowledge, the size of the sheet is the limiting factor here. The BR model has been shown to exhibit spiral wave activity around a linear core (Krinsky and Efimov, 1992; Efimov et al., 1995). However, in those simulations the 2-D matrix and the core itself were both larger than the array used here. Thus it should be noted that the LRI model may exhibit stationary activity in very large sheets.

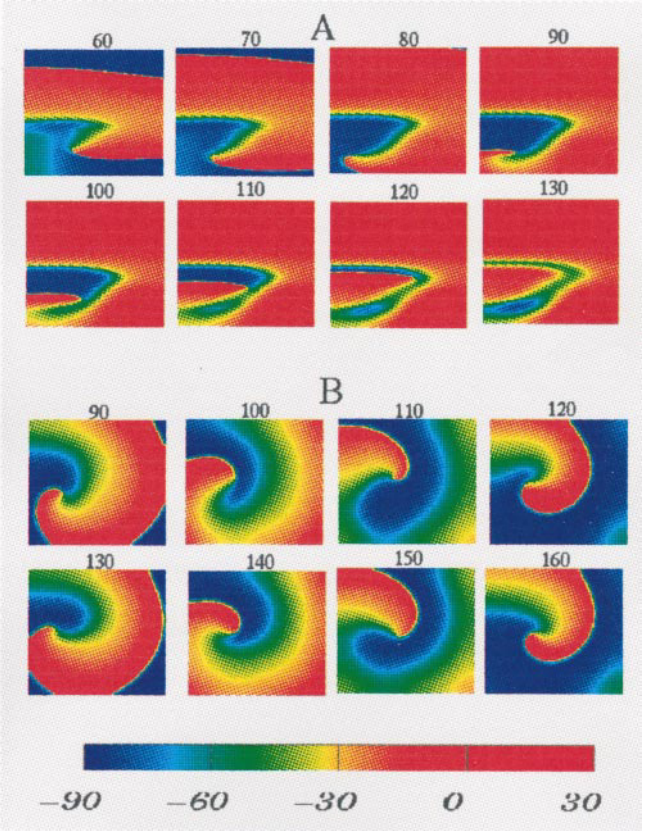

FIGURE 1 Initiation of spiral wave activity in an anisotropic cardiac sheet of 2 cm × 2 cm using the original LR model (*A*) and a modified model exhibiting a short APD (SAPD; *B*). Numbers at the top of each panel indicate the time after the S2 stimulus of the cross-field stimulation protocol. The color legend used to map the potential distribution (mV) is shown at the bottom.

Role of the kinetics of the activation front: the SAPD model

It seems reasonable to postulate that spontaneous spiral wave termination may be prevented by a rapid and sustained abbreviation of the APD of the premature (S2) wave. In fact, it is now well documented that APD can vary from a value of 300–400 ms at a long cycle length to ~150 ms (Elharrar and Surawicz, 1983; Robinson and Boyden, 1987) at high stimulation rates. Thus we performed a large number of simulations to test the hypothesis that accelerating the rate of APD adaptation to abrupt abbreviation of the activation frequency would accurately simulate stable spiral wave activity as seen previously in the experimental situation (Davidenko et al., 1991a; Pertsov et al., 1993). Not one of these tests was successful. We then performed additional simulations using a different model, the SAPD model. The objective here was to test whether increasing the area of recovered tissue ahead of the wave front would lead to stationary spiral wave activity. The SAPD model was derived from the LRI model simply by removing two of the currents activated during the plateau; i.e., the slow inward current (I_{si}) and the plateau potassium current (I_{Kp}). Furthermore, because patch-clamp experiments (Delmar et al., 1991; Ibarra et al., 1991) have shown that the inward rectifier (I_{K1}) is larger than that predicted by the formulation used in the LRI model (Beaumont et al., 1995b), we multiplied this formulation by a factor of 2. Simulations were carried out in a 2 cm × 2 cm sheet with an axial resistivity of 200 Ω-cm.

As shown in Fig. 1 *B*, the SAPD model is capable of sustaining spiral wave activity. The figure shows the evolution of the excitation pattern in space and time from 90 to 160 ms after cross-field stimulation. The reentrant excitation pattern was periodic and sustained. However, the rotation period (38 ms) was unrealistically short. Further reduction of the APD by increasing the conductance of I_K led to a proportional reduction in the rotation period, thus suggesting that, contrary to what happens in the experimental situation (Davidenko et al., 1991a; Pertsov et al., 1993), in the SAPD model there is no excitable gap, and the rotation period is determined primarily by the refractory period. Hence, in the face of these results and the large number of failures in attempting to reproduce stationary spiral waves by modifying the repolarization mechanism, we concluded that neither incorporation of a rapid APD adaptation mechanism nor abbreviation of APD by removing plateau currents would be sufficient to reproduce realistic spiral wave dynamics.

Exploring the parameter space of the SAPD model

From the foregoing it is clear that additional modifications would be needed in the SAPD model to obtain numerical simulations that could more accurately reproduce experimental results (Davidenko et al., 1990, 1991a,b; Pertsov et al., 1993). We hypothesize that the above discrepancies are caused by an inadequate definition of the kinetics of the activation front. Experimental results have shown the existence of a relatively large excitable gap (~50 ms) during stable spiral wave activity (Davidenko et al., 1990, 1991a,b; Pertsov et al., 1993; see Table 2). This implies that the activation front does not invade some excitable areas of the tissue, which can be achieved only when there is a very specific kinetics of the activation front.

To test the above hypothesis, we explored the parameter space of the SAPD model in regions affecting the kinetics of the activation front. We used the SAPD model because its brief APD allows sustained spiral wave activity in the 2 cm × 2 cm sheet. We elected to vary the following parameters: 1) the voltage threshold for activation of the impulse; 2) the maximum conductance of the sodium current (G_{Na}); and 3) an offset to the time constant of activation of the sodium current (ϵ_m; see Eq. 3). The voltage threshold for activation was changed by shifting by an amount, ψ_m, the voltage dependence of the functions that parameterize the steady-state open fraction of the sodium channel (see Eq. 3, parameter ψ_h).

In Fig. 2 we present an exploration of the parameter space (ψ_m, G_{Na}, and ϵ_m) of the SAPD model. The figure shows the trajectories followed by a reference point on a spiral wave during periods ranging from 500 ms to 2 s. The reference corresponds to the null curvature point on the −30 mV isopotential (see Appendix for details and justification). Our objective here was to show the existence of parametric conditions where a relatively large stationary core and excitable gap could be observed. It would be beyond the scope of this study to present a detailed structure of the parameter space. The number of simulations involved in the precise determination of each boundary would be out of reach. However, for the sake of the presentation, we identify zones in the parameter space. Although the boundaries are rough estimates, it is informative to note the existence of zones of different behaviors and how the transition to a stationary core is achieved in this model. Overall, the figure shows that, under control conditions, the core undergoes a meandering pattern (zone h) with large loops (a rotating ellipse). When the excitability is increased above the nominal value, the behavior becomes chaotic (zone c). Reducing excitability below control produces meandering (zones h, e, and d). However, if this is done in a certain manner, lowering excitability can in fact yield a stationary core (zone s). A large reduction of excitability creates conditions in which planar waves can, but curvilinear waves cannot propagate (zone b), which means that it is not possible to induce spiral waves in this zone. Such a situation has been reported previously for the FitzHugh-Nagumo model (Winfree, 1991). The meandering zone is subdivided into three types of patterns: hypocycloidal (h), epicycloidal (e), and daisy (d). Hypocycloidal and epicycloidal patterns were also reported for the FitzHugh-Nagumo (Winfree, 1991; Barkley, 1994) as well as the Beeler and Reuter model (Efimov et al., 1995). The daisy pattern is a hypocycloidal pattern, but has been labeled differently for other reasons that should become obvious below.

The most interesting result presented in Fig. 2 is the fact that changes in ψ_m and ϵ_m potentiate each other, such that relatively small changes in these parameters can yield a

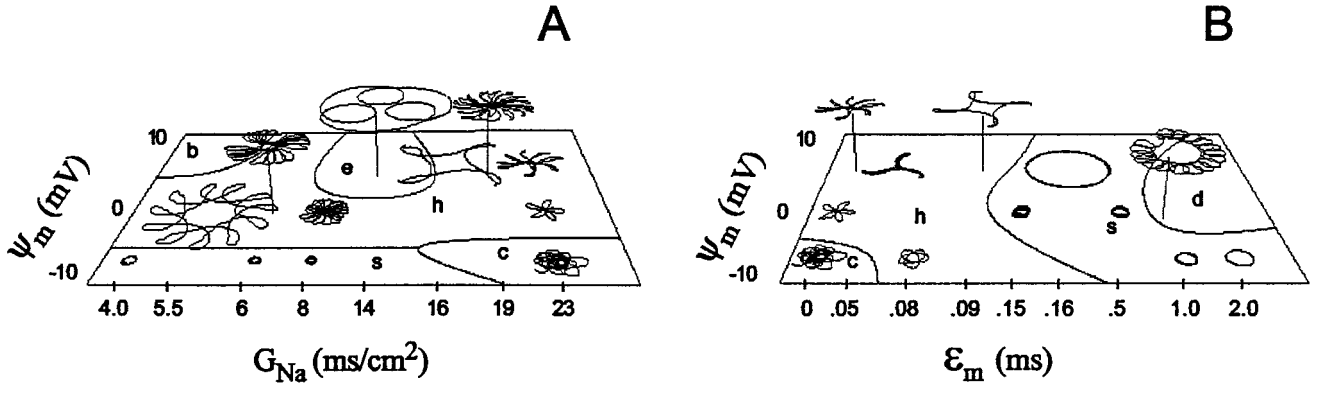

FIGURE 2 Patterns of spiral wave meandering in the SAPD model during sustained spiral wave activity as seen on the parameter space. The meandering patterns were obtained by tracking the trajectory of the null curvature point as measured on a −30-mV isopotential. The figure shows meandering patterns obtained when we varied the shift in the voltage dependence of the gating mechanism (ψ_m), the conductance of the sodium current (G_{Na}), and an offset to the time constant for activation of the sodium current (ϵ_m). For the sake of presentation, the horizontal axis of each plane is stretched in a nonlinear manner, and the patterns are scaled by a factor of 1.5. Some patterns are raised above the plane to avoid overlapping of the traces. In these cases, a line joins the center of each pattern to its origin on the parameter space. Overall, these patterns enable the distinction of five different regions in the parameter space, exhibiting stationary cores (s), chaotic behavior (c), block of curvilinear waveforms, hypocycloidal meandering patterns (h and d), and epicycloidal meandering patterns (e). See text for more details.

large stationary core. At G_{Na} = 23 mS/cm^2, ψ_m = 10 mV, and ϵ_m = 0.16 ms, the propagation velocity is 33 cm/s, the core is ~7 mm in diameter, and the rotation period is 115 ms, which produces an excitable gap of ~70 ms. Such behavior is consistent (in terms of core size and excitable gap) with experimental results. Stationary cores were also produced in other conditions (zone s), but they were very small and the spiral did not exhibit a significant excitable gap. There are two important issues to consider at this point. First, for the parameter range explored in Fig. 2, we did not observe significant changes in APD. Therefore the different meandering patterns presented are essentially the result of changes in the kinetics of the activation front. Second, we could observe a large circular core only when $(dV/dt)_{max}$ was significantly reduced. For the largest circular core presented in Fig. 2, $(dV/dt)_{max}$ was 60 V/s. The implications of this are discussed below under Limitations of the Model.

The transition from meandering to stationary circular cores requires additional discussion. When the parametric conditions are close to those that produce a stationary core, the meandering pattern should exhibit loops that are almost circular. This can be appreciated by observing the pattern shown in zone d. Under these conditions, an interaction between the spiral tip and the repolarization tail occurred before the spiral completed a rotation. After this interaction, the spiral tip exhibited a large excursion before drawing another loop. When the spiral could complete a rotation without such interaction, the pattern was circular and stationary. A similar transition has previously been documented for the FitzHugh-Nagumo model (Barkley, 1994). The other locus of interest is the boundary of zone e, because when approaching this zone, the global size of the meandering pattern should increase. For topological reasons, the transition from an epicycloidal to a hypocycloidal pattern should occur through a cycloidal pattern. Examples of such a transition have been documented for the FitzHugh-Nagumo (Barkley, 1994; this author also presented a mathematical analysis of the transition) and Beeler and Reuter (Efimov et al., 1995) models. Because a cycloidal pattern has an infinite orbit, the main orbit of the meandering pattern should increase smoothly when approaching this zone.

It is interesting that these findings agree reasonably well with previous suggestions made by the kinematic theory (Mikhailov and Zykov, 1991), which postulates that the core size and the frequency of rotation are inversely proportional to the critical radius for propagation. We obtained a large stationary core when we significantly reduced excitability and upstroke velocity, which also causes a reduction of the critical radius of curvature for sustained propagation. This effect may also be explained in terms of the analysis presented more recently by Starobin et al. (1996), whereby the conditions for the core formation are related to the balance of currents between the activation front and adjacent recovered areas.

Stationary spiral wave activity in an anisotropic membrane model: the Shina model

Ionic properties of the model

The results of the previous section suggest that, under appropriate parametric conditions, a membrane model can undergo rotating spiral wave activity around an unexcited core. Therefore the question arises as to whether it is possible to simulate spiral wave activity in a small 2-D array when the action potential model closely resembles the experimentally recorded action potential. To answer such a question, we carried out additional simulations using a new modification of the LRI model, as follows: 1) we replaced the sodium current by the formulation that enabled us to obtain a large stationary core with the SAPD model (see Fig. 2, ψ_m = 10 mV, ϵ_m = 0.16 ms, G_{Na} = 23 mS/cm^2); 2) the inward rectifier, I_{K1}, was multiplied by 2 (see Role of the Kinetics of the Activation Front for justification); 3) the slow inward current I_{si} was divided by 2 to obtain a realistic action potential morphology (Ibarra et al., 1991); and 4) the delayed rectifier (I_K) was updated using a formulation that exhibits milder rectification (Matsuura et al., 1987). Hereafter we refer to this new model as the Shina model (used in all subsequent simulations). According to the results presented in the previous section, modifications to the kinetics of the activation front are required to obtain a stationary core. Other modifications were required to approximate the behavior of the cell response during rapid pacing and to produce an appropriate distribution of refractoriness, which is essential for spiral wave initiation. For example, reducing APD in the LRI model just by increasing the conductance of I_K produces a large refractory interval after full repolarization, which is not realistic (i.e., it has not been documented for ventricular cells). This phenomenon, in fact, prevents initiation of spiral waves in a small sheet of cells when cross-stimulation is used. In the remainder of the paper, we present simulations using models exhibiting various APDs obtained by changing the conductance of the delayed rectifier (G_k). For the sake of presentation, we refer to each model by the term Shina, followed by the value of G_k. Thus, for example, Shina⟨Gk75⟩ means that we used a conductance of 75 mS/cm^2 (see Table 3). Unless otherwise indicated, the simulations were carried out using an anisotropic sheet (anisotropy ratio 4:1) of 2 cm × 2 cm. The resistivities in the longitudinal and transverse directions were, respectively, 200 Ω-cm and 3200 Ω-cm for the anisotropic sheet and 200 Ω-cm for the isotropic sheet.

Spiral wave activity in Shina

Fig. 3 shows the time course of spiral wave activity obtained using the models Shina⟨Gk75⟩ (Fig. 3 *A*) and Shina⟨Gk10⟩ (Fig. 3 *B*). In each case, the electrical activity lasted 1 s, which was sufficient to establish stationary motion. The stability of the excitation pattern can be appreciated in the traces of Fig. 4, which shows the potential in time at a few selected points. The activity in Fig. 3 *A* is strikingly similar

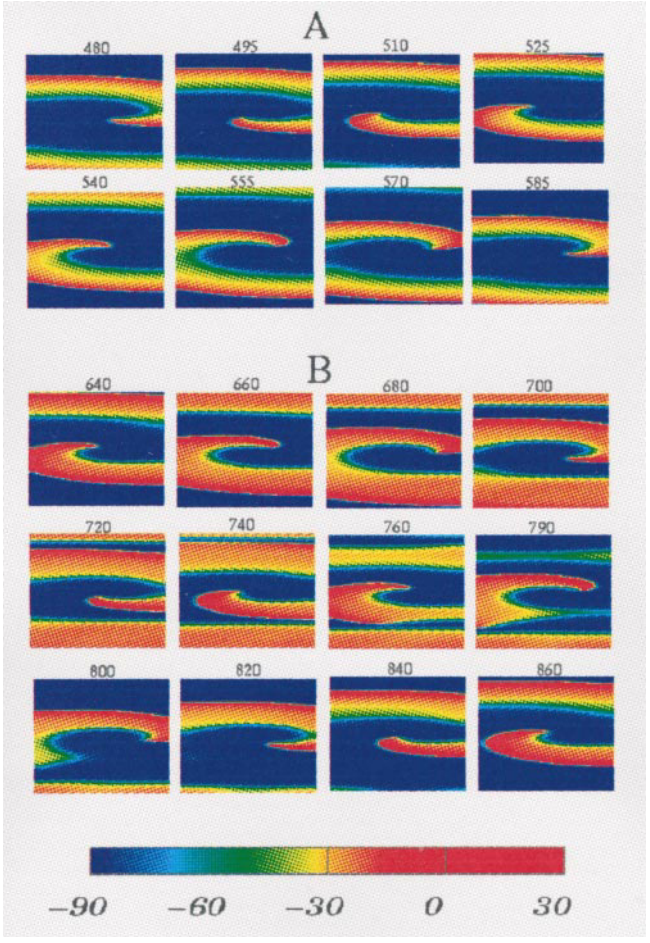

FIGURE 3 Spiral wave activity in 2 cm × 2 cm anisotropic cardiac sheets (ratio of longitudinal to transverse velocity is 4:1), according to a full action potential model exhibiting a refractory periods of 147 ms (*A*) and 235 ms (*B*). In *B* the refractory period during plane wave activation is about twice as long as the rotation period. As a result, whereas there is 1:1 activation near the center, the activation pattern in the periphery is 2:1. Numbers at the top of each panel indicate the time after the S2 stimulus in the cross-field stimulation protocol. The color legend used to map the potential distribution (mV) is shown at the bottom.

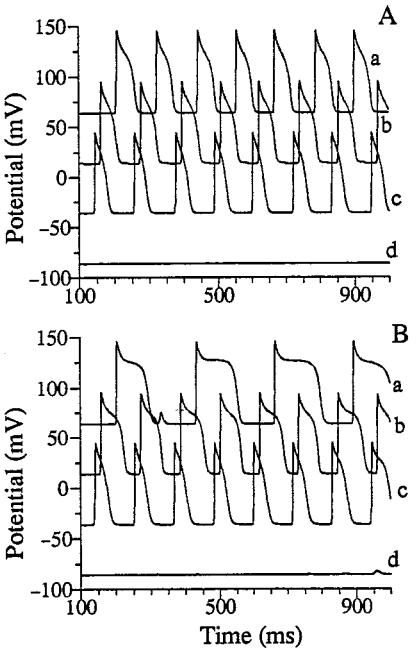

FIGURE 4 Time course of membrane potential changes recorded at various sites during spiral wave activity. Traces in *A* and *B* were obtained during spiral wave activity in the simulations shown, respectively, in Fig. 3, *A* and *B*. Tracings correspond to individual points aligned vertically on an imaginary line at the center of the 2 cm × 2 cm domain. The points are at 0.2 cm (*trace a*), 0.6 cm (*trace b*), 0.8 cm (*trace c*), and 1 cm (*trace d*, which is within the core) from the upper border. Each trace is offset by 50 mV with respect to its immediate neighbor in the display.

to that observed in previously published experimental examples (Davidenko et al., 1991a,b; Pertsov et al., 1993; see also Table 2). Furthermore, it is remarkable that the spatial extent of the excited state (i.e., the wavelength; red to light blue) was quite small in a relatively large area in the vicinity of the center of rotation. Because, during spiral wave activity, the activation front merges with the repolarization tail near the spiral tip (see Fig. 8 in the Appendix), one would have expected shortening of APD only in a small area surrounding the tip. However, the spatial extent of the APD abbreviation was unexpectedly large. Because the excitable gap was also relatively large (~55 ms), the tissue was fully recovered before invasion by the activation front, very close to the center of rotation. Full excitability near the core is also apparent from the fact that the amplitude of the impulse is practically normal as close as 2 mm from the center of rotation (Fig. 4 *A*, *trace c*). Therefore, there is apparently no obvious reason to expect an abbreviated response beyond that small radius. To better understand this phenomenon, we induced spiral waves in the 2-D Shina⟨Gk10⟩ model, which exhibits an APD that is about twice as large as that of Shina⟨Gk75⟩ (see Table 3).

As shown in Fig. 3 *B*, although the wavelength of Shina⟨Gk10⟩ (as measured during planar wave propagation) was larger than the size of the preparation, it was still possible to obtain stationary spiral waves whose APDs were distributed radially over the entire preparation. In fact, the data in Figs. 3 *B* and 4 *B*, taken from the same simulation, demonstrate a striking shortening of APD and wavelength

TABLE 2 Electrophysiological measurements of spiral wave activity

Characteristic	Value	Reference
Rotation period (ms)	183	Davidenko et al. (1991b)
	142–200	Davidenko et al. (1990)
	117–250	Pertsov et al. (1993)
S1–S2 (ms)*	130–140	Davidenko et al. (1990)
Ts/Tr[#]	1.39	Davidenko et al. (1991b)
	1.39	Pertsov et al. (1993)
Core (mm)	3.1 × 5.5	Davidenko et al. (1991b)
	3–5	Davidenko et al. (1990)
	1.3–4 × 2.7–11	Pertsov et al. (1993)

*Coupling interval used to initiate spiral waves.
[#]Ratio of the rotation period of the spiral (Ts) over the refractory period (Tr) measured during planar wave at a similar cycle length.

TABLE 3 Characteristics of the membrane models used in the study

Characteristics*	Shina⟨gk75⟩	Shina⟨gk10⟩	LRI
Longitudinal propagation velocity (cm/s) for solitary impulse	33	33	74
$APD_{90\%}$ for solitary impulse (ms)	120	220	366
Refractory period for solitary impulse (ms)[#]	147	235	382
Wavelength for solitary impulse	4.85	7.75	28
$(dV/dt)_{max}$ for solitary impulse (V/s)	60	60	240
Rotation period for spiral wave (ms)	115	115	Not applicable
Current threshold ($\mu A/cm^2$)[§]	15	15	10

*The calculations were made with an axial resistivity of 200 Ω-cm.
[#]The refractory period is calculated with a stimulus 1.5 times threshold.
[§]The stimulus was applied on 2 mm, for a 5-ms duration.

near the center of rotation. In this case, the rotation period was also 115 ms. However, the excitation pattern was more complex. Whereas at the center there was 1:1 activation, only one of every two wave fronts reached the upper and lower borders of the array. Indeed, at 720 and 740 ms, two clearly delineated lines of conduction block were apparent, one at the top third and the other at the bottom third of the array. The block of conduction in the periphery was consistent with the long refractory period measured in the cable configuration. However, the stability of the kernel of electrical activity revolving in a confined region around the center of rotation was unexpected. We found that this was possible because of the existence of a significant shortening of the wavelength in this region. As shown by trace c of Fig. 4 *B*, this kernel of activity was very stable. Consequently, there were different rates of activation at either side of each line of block.

Spatial distribution of the wavelength in Shina

During spiral wave activity the propagation velocity changes all along the activation front because of changes in curvature. This may explain the reduction of wavelength observed around the center of rotation (Fig. 3). The slow propagation velocity close to the center of rotation certainly contributes to wavelength abbreviation. However, our measurements of the spatial distribution of APD show that the abbreviation of the wavelength is primarily the result of APD abbreviation. Fig. 5 shows graphs of APD distribution measured on a set of points aligned vertically along an imaginary line joining the center of rotation to the upper border of the array. APD distributions were compared for models exhibiting APDs of 120 ms (shina⟨Gk75⟩) and 220 ms (shina⟨Gk10⟩), using either an anisotropic (resistivity 200 Ω-cm by 3200 Ω-cm) or an isotropic cardiac sheet (200 Ω-cm). In our measurements we considered only impulses exhibiting an amplitude larger than 65 mV. Curves b and c indicate the existence of cycle-to-cycle APD alternation near the line of transition between 1:1 and 2:1 activation (i.e., the line of block). As the impulse entered a more refractory zone, its duration and amplitude decreased, and eventually the impulse stopped at the line of block. The next impulse was able to reach the periphery. As indicated by the plateau of trace c, the propagated impulse is influenced by the behavior of the preceding blocked impulse. The block creates a zone of partial refractoriness that reduces the rate of change of APD as the wave moves away from the center of rotation.

The largest APD distribution occurred for Shina⟨Gk10⟩ in the anisotropic cardiac sheet (*trace c*, Fig. 5). The APDs ranged from 45 to 130 ms over a distance of 1 cm in the transverse direction (equivalent to 4 cm along the longitudinal direction). Yet APD did not reach saturation value (220 ms). Curve d, obtained using the same model but now in an isotropic preparation, indicates that similar results may be obtained even in the absence of conduction block. In summary, the system is very stable, the spiral rotates at a fixed frequency, and, if the unexcited core is sufficiently large, depending on the APD (for a solitary wave), there can be a very large radial distribution of the wavelength caused by a radial distribution of APD.

Electrotonic influence of the unexcited core

Our interpretation of the above data is that APD abbreviation results from a powerful electrotonic (current sink) effect exerted by the core. During spiral wave activity, while cells in the periphery are depolarized periodically by the passage of the electrical impulse, cells in the core remain unexcited near the resting value (*bottom traces* in Fig. 4, *A* and *B*). Consequently, a large potential gradient is established that produces a strong radial current flowing from the periphery toward the core. To provide further credence to the idea that APD abbreviation is the result of a potential gradient established by the core, we studied the electrotonic influence of an unexcited core in a disk of radius 1 cm. The unexcited core was simulated by a small region (radius 3 mm) in which the membrane contained only the I_{K1} channel. The model shina⟨Gk10⟩ was used for the rest of the disk. The axial resistivity was 3200 Ω-cm. We simulated periodic stimulation from an external source (applied from 3–4 mm; pulse duration 5 ms; pulse amplitude 15 $\mu A/cm^2$; cycle length 120 ms) at the interface between the excitable and unexcitable zones. After stimulation, the electrical impulse propagated through the excitable zone, but could not penetrate the unexcitable region. Therefore, under these conditions, a regenerative response moved away from a large depolarized region. This configuration enabled us to

observe APD abbreviation over a large distance similar to what was observed during spiral wave activity (see above).

In Fig. 6 we compare the time course of the membrane potential changes in a uniform (stimulus was applied at the center) and a nonuniform (as described above) disk during the application of repetitive stimulation. In each configuration the tracings correspond to sites located at 4 mm and 9 mm from the center. As shown in Fig. 6 *A1*, in the uniform disk, single excitation waves propagated radially toward the periphery and yielded action potentials of similar duration. In contrast, as shown in Fig. 6 *A2*, in the nonuniform disk, the influence of the unexcitable region was sufficient to abbreviate significantly the APD up to ~1.0 cm from the center of the disk. In the two recordings shown, the APD of the cell located 4 mm from the center was most affected. In Fig. 6, *B1* and *B2*, are shown the responses to repetitive stimulation at a cycle length of 120 ms. In the uniform case (Fig. *B1*), although the electrical activity was irregular, there was uniform n:n (stimulus:response) activation throughout the disk. On the other hand, in the nonuniform disk (Fig. *B2*), the excitation pattern was discontinuous. In this case, because APD increased as the impulse moved away from the unexcitable zone, the diastolic interval between two consecutive beats decreased with distance from the unexcitable zone. At a critical distance (~7 mm), the diastolic interval was so short that an impulse was blocked, but the subsequent impulse could propagate up to the border of the disk. As a result, near the center one observes a 1:1 activation pattern (after transients), whereas, in the periphery, the pattern was 2:1. In other words, the repolarizing influence exerted by the passive region led to sufficient abbreviation of APD near the interface, which enabled 1:1 capture at a high frequency of stimulation. Beyond a line of block at ~7 mm, 1:1 capture was no longer possible. Overall, this effect is comparable to the one demonstrated in Figs. 3–5 for spiral wave activity.

It seems counterintuitive that an electrotonic effect may have an influence at a distance that is much larger than the space constant. In fact, the large spatial extent of such an influence is possible because it takes place between neighboring cells during propagation of the electrical impulses. Close to the core, the potential gradient at the level of the wave tail is very large and the APD abbreviation is proportional to an axial current (electrotonic current) produced by the potential gradient. The cells that are activated earliest near the core are prematurely repolarized because of the electrotonic influence exerted by the core itself, which remains unexcited (i.e., cells within the core remain very near their resting potential). These cells also abbreviate the APD of the cells activated just a few milliseconds later because they are separated from them by only a few millimeters along the radial direction. The premature repolarization of such cells creates a strong potential gradient during the repolarization phase of cells activated yet a few milliseconds later, which in turn abbreviates their APD. Thus the APD abbreviation influence is transmitted from cell to cell with attenuation as the impulse propagates toward the periphery. Overall, our results strongly support the mechanism proposed above, namely, that APD abbreviation during spiral wave activity is a consequence of the electrotonic influence exerted by the core on its immediate surroundings, which in turn influence APDs in more peripheral regions.

Is the unexcited core excitable?

It is important to note that during stationary spiral wave activity the center of rotation, the core, while unexcited, remains excitable at all times. To provide definite proof that this is indeed the case, an additional simulation was done in a 4 cm × 4 cm isotropic sheet with an axial resistivity of 200 Ω-cm. Spiral wave activity was initiated and allowed to stabilize (i.e., 10 rotations). Subsequently, a 5-ms stimulus of 20 μA/cm^2 (threshold 15 μA/cm^2) was applied to an area of 2 mm × 2 mm within the core. In Fig. 7 we present 3-D plots of three different snapshots of the excitation pattern 2, 10, and 20 ms after application of the stimulus. In all frames, the membrane potential is represented along an axis perpendicular to the plane of the sheet. It is clear that the stimulus generated an active response. At 20 ms, this response began to merge with the electrical impulse revolving around it. From the shape of the resulting pattern, one may predict that the spiral wave activity would not be terminated by such a stimulation, because there is still a large amount of excitable tissue in front of the activation front. In fact, as

TABLE 4 Electrophysiological measurements of planar waves on isolated preparation of sheep epicardium

Characteristics	BCL*	Longitudinal	Transverse	Reference
Propagation velocity (cm/s)	500 alt.	34	11	Delgado et al. (1990)
	1000	50	9	Delgado et al. (1990)
	300	25	4	Pertsov et al. (1993)
	~400	40	20	Davidenko et al. (1990)
	750 alt.	60	13.5	Delmar et al. (1987)
Maximum upstroke velocity (V/s)	1000	140	180	Delgado et al. (1990)
	1000	129	167	Delgado et al. (1990)
	750	120	140	Delmar et al. (1987)
APD_{90} (ms)[#]	1000	205	208	Delgado et al. (1990)
Refractory period (ms)	1000	191	215	Delgado et al. (1990)

*Basic cycle length at which the measurement was made.
[#]Action potential duration measured at 90% repolarization.

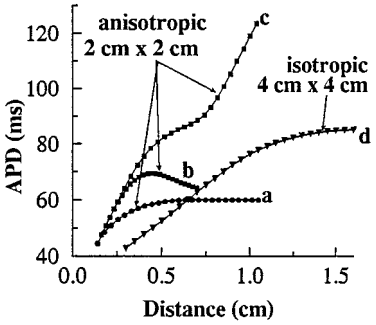

FIGURE 5 Spatial distribution of action potential duration at various locations along an imaginary line joining the center of rotation to the upper border of the domain. Measurements were performed during spiral wave activity obtained using two different models under two different conditions. Trace a corresponds to model Shina⟨Gk75⟩ on an anisotropic sheet; traces b and c correspond to model Shina⟨Gk10⟩ on an anisotropic cardiac sheet (here two traces are required because APD alternates close to the center of rotation); trace d corresponds to model Shina⟨Gk10⟩ on a 4 cm × 4 cm isotropic sheet.

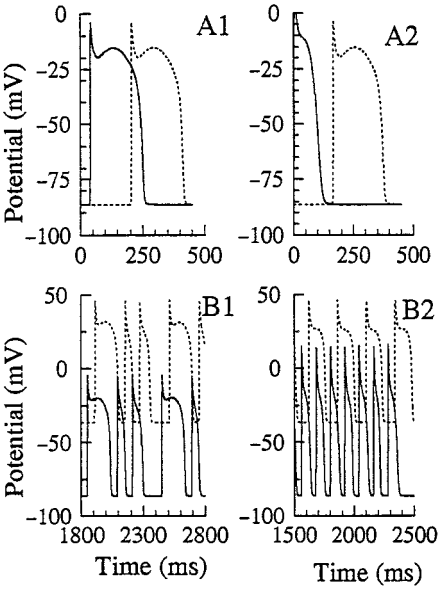

FIGURE 6 Time course of membrane potential changes in a disk of cardiac model cells during external periodical pacing. The recording sites were 4 mm (————) and 9 mm (· · · · · ·) from the center. (*A1* and *B1*) Uniform disk. (*A2* and *B2*) Nonuniform disk. The latter has a central region with a radius of 3 mm containing only I_{K1}. *A1* and *A2* correspond to a single electrical stimulus, whereas *B1* and *B2* were obtained during repetitive stimulation at a cycle length of 120 ms. In *B1* and *B2*, traces are offset by 50 mV with respect to their immediate neighbor in the display. See text for further details.

predicted by FitzHugh-Nagumo simulations (Davidenko et al., 1995), stimulation at the core resulted in a shift of the rotating activity with the formation of a new core (not shown). Nevertheless, the results demonstrate that during stationary spiral wave activity, the core remains excitable.

DISCUSSION

Summary of model predictions

This study yielded two important new findings. First, the formation of an unexcited core in an ionic model of cardiac cells depends primarily on the kinetics of the activation front. Second, once formed, the unexcited core exerts a substantial electrotonic influence on the surrounding tissue. The latter finding is supported by previously published experimental results. For example, it is well known that healthy myocardium can sustain very rapid tachycardias (Cha et al., 1994; Gray et al., 1995; Boersma et al., 1994) at cycle lengths that are shorter than the refractory period, as measured during external stimulation. Specifically, a difference of 21 ms between the functional refractory period and the cycle length of the tachycardia has been reported for rabbit heart (Boersma et al., 1994). Electrotonically mediated abbreviation of APD produced by the unexcited core offers a robust explanation for this and for the mechanism by which spiral waves can rotate at very large frequencies in cardiac muscle.

Based on our simulation results, the following specific testable predictions can be made: 1) During vortex-like activity, there should be a radial distribution of APD. 2)

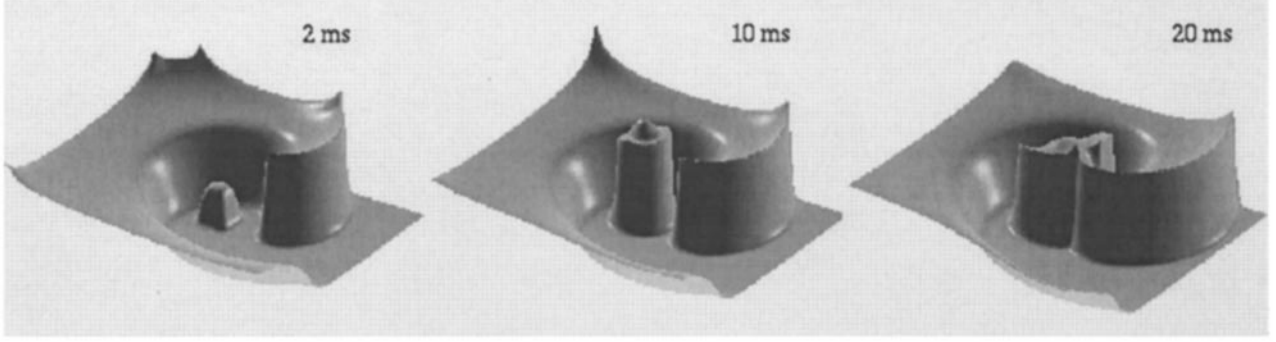

FIGURE 7 Demonstration that the spiral wave core is excitable. The membrane potential is represented along the axis perpendicular to the plane of the sheet. The spiral was initiated by cross-field stimulation using the model Shina⟨Gk10⟩. Once stationary activity was reached, a single stimulus (20 μA/cm^2, 5-ms duration) was applied at the center of rotation to an area of 2 mm × 2 mm. Left to right: 3-D plots of potential distribution in space 2, 10, and 20 ms after application of the stimulus.

Programmed stimulation involving the use of a train of stimuli (S1) at constant cycle length followed by a premature beat (S2) should, under appropriate conditions, result in the initiation of reentry with formation of the core. Initially, an area of conduction block will exist at an appreciable distance from the core. However, block may be transient, because the rapid stimulation imposed by the kernel of activity near the core may produce, over some finite period of time, APD abbreviation, which will allow for 1:1 capture all over the excitable domain. 3) During stable spiral wave activity, the functional refractory period measured in the immediate vicinity of the core should be consistently briefer than that measured at the periphery and that measured during pacing at stimulus rates equivalent to the rotation frequency.

Limitations of the model

None of the model versions used here incorporate mechanisms for the regulation of ionic concentrations, which may be considered a drawback, given the existence of newer, more elaborate models than LRI. However, we feel that our approach is a good trade-off between computational expense and description of the membrane kinetics. Moreover, our major concern with the use of complex models such as those of Nordin (1993), Noble (1990), and Luo and Rudy (1994), version II, is that they are based on an appreciable number of empirical components. Indeed, the construction of these models depends heavily on the ability to fit model parameters of individual ionic currents. There are two major problems with that approach. First, the model parameters that one can extract by fitting experimental data are usually not unique (Beaumont et al., 1993). Second, there are significant errors in the parameter values because of experimental limitations and the numerical procedures used to estimate the model parameters. Both factors severely impair the quality of the model predictions. For example, our study demonstrates that minor changes in the kinetics of the activation front can significantly change the prediction of the model (e.g., from meandering to stationary spiral wave activity). It would be very difficult to generate, with sufficient accuracy, all of the experimental data required to determine in a realistic manner the kinetics of the activation front.

Both the scientific method adopted in this study and the results obtained strongly suggest that knowledge of the role of the model parameters in determining a particular behavior is an essential prerequisite for the appropriate use of experimental data in the construction of a membrane model. This information determines the accuracy with which different aspects of the current kinetics should be known. This suggestion finds an additional justification in the fact that, with the exception of the j-gate, the sodium current model used in the LRI model was obtained from experiments performed in chick embryonic cells (Ebihara and Johnson, 1980). Although it is now well documented that the sodium current kinetics change significantly during embryonic development (Fujii et al., 1988), before the parameter space of the membrane model was explored, there was no reason to suspect a priori that changes in the current kinetics occurring during embryonic development may have such important consequences for the model predictions.

Stationary spiral wave activity was obtained using a membrane model whose upstroke velocity was 60 V/s, which is much lower than the value observed in experiments under physiological conditions (Kodama et al., 1995; Muruyama et al., 1995). For example, in thin sheep ventricular epicardial muscle, $(dV/dt)_{max}$ has been reported to be ~120 and ~180 V/s during longitudinal and transverse propagation (see Table 4). In papillary muscles $(dV/dt)_{max}$ is ~200 V/s (Kodama et al., 1995; Muruyama et al., 1995), whereas, in single ventricular myocytes, values as low as 80 V/s and as high as 600 V/s have been reported (Hume, 1985; Kodama et al., 1995; Muruyama et al., 1995), depending on the temperature and the stimulation protocol. We have carried out a large number of simulations in our efforts to find the appropriate conditions for the upstroke velocity that lead to sustained spiral wave activity. Our results strongly suggest that only membrane models with relatively small upstroke velocity values are capable of sustaining such activity. This result is problematic, because spiral wave activity, as well as other vortex-like reentrant activity involving the formation of an unexcited core and excitable gap, has been demonstrated in structurally normal heart under physiological conditions. We feel that an important limitation of the model used here is that it does not show an appropriate frequency dependence of $(dV/dt)_{max}$. As we see it, such a frequency dependence has been essential to the ability of previous investigators (Davidenko et al., 1990, 1991a,b; Pertsov et al., 1993; Zhou et al., 1992; Cha et al., 1994) to initiate sustained spiral wave activity in experimental preparations by means of high-frequency pacing or premature stimulation. Although we did not systematically test all models of ventricular cells (except LR phase I and BR), we do not have any reason to believe that such a mechanism is incorporated into existing models, at least to an extent that allows formation of stationary spiral waves. Hence one of the major conclusions to be drawn from this study is that further improvements of membrane models attempting to accurately reproduce functional reentrant activity must involve careful attention to and improvements of the frequency dependence of $(dV/dt)_{max}$ and conduction velocity.

Implications for therapy for life-threatening arrhythmias

The therapeutic goal of lengthening APD and, consequently, the refractory period needed to terminate reentrant tachycardias is widely accepted (Colatski, 1992; Hondeghem, 1994). This assumption follows very naturally from our understanding of the functions and interactions of the membrane components involved in the genesis of the

action potential. A previous simulation study using the FitzHugh-Nagumo model (Starmer et al., 1995) challenged this concept by suggesting that lengthening APD results in meandering of the spiral wave rather than its termination. Our simulation results also suggest that lengthening APD will not terminate spiral wave (see Fig. 3 *B*). However, the mechanism of action is different. When the spiral wave rotates around a large unexcited core, the electrotonic influence of the latter could significantly counterbalance the action of agents whose action is to prolong APD (e.g., class III drugs). Indeed, in Fig. 3 we have shown that spiral waves are sustained by two membrane models that differ from each other in the conductance of the potassium current and thus the duration of the refractory period. One model had a refractory period about twice as large as the other. Yet both exhibited the same cycle length (115 ms) during spiral wave activity. This suggests that if a purely class III drug effect is exerted on the model with the shorter refractory period after establishment of stable reentry, an effect that is strong enough to double the refractory period would still be insufficient, and the spiral wave activity will continue, apparently undisturbed. Our results lead us to speculate that a combined drug action of increasing excitability and prolonging refractory period would have a better chance of antiarrhythmic success.

APPENDIX: CALCULATION OF CURVATURE ALONG ISOPOTENTIALS

Using a finite-element method (FEM), the numerical solution is known in the form of a piecewise two-dimensional polynomial defined on a rectangular grid. For each quadrilateral element of the grid, a local isopotential segment is obtained from the intersection of the membrane potential with a constant plane at potential V_0. The isopotential segments are obtained in random order by scanning the quadrilateral elements of the grid. Then in a subsequent phase they are linked to form continuous curves.

Calculation of the curvature requires the representation of the isopotential line in a parametric form, which allows for the calculation of a continuous second derivative. This was obtained by fitting a smoothed cubic parametric spline to the set of points $\bar{x}_j, \bar{y}_j$, formed by the intersection of the isopotential segments with the sides of the rectangular elements of the grid. The chord joining these points serves as a reference axis, and the distance μ along this chord is the reference parameter of the parametric formulation. The coefficients b_j and c_j of the cubic parametric splines,

$$x(\mu) = \sum_{n=0}^{n=N} x^n(\mu), \qquad x^n(\mu) = \begin{cases} \sum_{j=0}^{j=3} b_j \mu^j & \text{for } \mu_n < \mu > \mu_{n+1} \\ 0 & \text{elsewhere} \end{cases} \tag{A.1}$$

$$y(\mu) = \sum_{n=0}^{n=N} y^n(\mu), \qquad y^n(\mu) = \begin{cases} \sum_{j=0}^{j=3} c_j \mu^j & \text{for } \mu_n < \mu > \mu_{n+1} \\ 0 & \text{elsewhere} \end{cases} \tag{A.2}$$

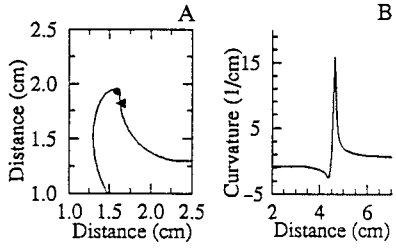

FIGURE 8 (*A*) −30 mV isopotential during spiral wave activity. The black circle indicates the point of maximum curvature, and the black triangle the point of null curvature. (*B*) Measurement of curvature along that isopotential. The distance in *B* is measured along the isopotential line.

are calculated by minimizing the following functional:

$$J(\mu) = \sum_{k=0}^{k=K} (x(\mu_k) - \bar{x}_k)^2 + \lambda \int_{\mu=0}^{\mu=L} \left(\frac{d^2 x(\mu)}{d\mu^2} \right)^2 d\mu + \sum_{k=0}^{k=K} (y(\mu_k) - \bar{y}_k)^2 + \lambda \int_{\mu=0}^{\mu=L} \left(\frac{d^2 y(\mu)}{d\mu^2} \right)^2 d\mu \tag{A.3}$$

where L is the length of the chord, K is the total number of intersection points along the chord, and the parameter λ indicates the stiffness of the curve. For all calculations, λ was fixed at 10^{-3}. This allowed for a smooth representation of the curve without jumps in the derivative at intersection points along the chord. The numerical solution of Eq. A.3 leads to a matrix system (Lancaster and Salkauskas, 1990), which is solved using a LU factorization technique. On the cubic parametric spline, the curvature $\kappa(\mu)$ is calculated by

$$\kappa(\mu) = \frac{(r'' \cdot r'')(r' \cdot r') - (r' \cdot r'')^2}{(r' \cdot r')^{3/2}} \tag{A.4}$$

where $r(\mu)$ is the radius vector joining the origin of the x-y axis system to a point $x(\mu)$, $y(\mu)$, along the parametric curve. The primes in the above equation denote the derivative with respect to μ. The reader can find details about the development of Eq. A.4 in Kreyszig (1972) or any basic textbook on differential geometry. An example of the calculation of curvature is provided in Fig. 8. The curvature was measured along a −30-mV isopotential taken on a spiral wave. To trace the trajectory followed by a spiral wave we used, as a reference point on the spiral, the point of null curvature taken on a −30-mV isopotential. Obviously, such a procedure implies some degree of arbitrariness in the size of the meandering patterns, which is unavoidable. However, using a −30-mV isopotential level minimizes this effect. At this level (about half-amplitude), the isoppotentials are close to each other. Therefore a change in the isopotential level results in a minimal change in the size of the meandering pattern. Furthermore, the position of the null curvature point is not very sensitive to slight changes in the wave shape. This is not the case for other characteristic points, like the point of maximum curvature.

We are grateful to Drs. Marcel Wellner, Guillermo Calero, Omer Berenfeld, and Arkady Pertsov for fruitful discussions and Andrew Goodwin for technical assistance. We thank the staff of the Cornell Theory Center at Cornell University for the support provided during this study.

Supported in part by Grants P01-HL39707, R01-HL29439, and R01-HL46148 from the National Heart, Lung and Blood Institute, National Institutes of Health. JMD is an Established Investigator of the American Heart Association.

REFERENCES

Barkley, D. 1994. Euclidian symmetry and the dynamics of rotating spiral waves. *Phys. Rev. Lett.* 72:164–167.

Beaumont, J., N. Davidenko, J. Davidenko, and J. Jalife. 1995a. Self-sustaining spiral wave in a two-dimensional ionic model of cardiac ventricular muscle. *In* Computer Simulations in Biomedecine. H. Power and R. T. Hart, editors. Computational Mechanics Publications, Southampton and Boston. 75.

Beaumont, J., D. C. Michaels, M. Delmar, J. Davidenko, and J. Jalife. 1995b. A model study of changes inexcitability of ventricular muscle cells: inhibition, facilitation and hysteresis. *Am. J. Physiol.* 268 (*Heart. Circ. Physiol.* 37):H1181–H1194.

Beaumont, J., F. A. Roberge, and L. J. Leon. 1993. On the interpretation of voltage-clamp data using the Hodgkin-Huxley model. *Math. Biosci.* 115:65–101.

Beeler, G. W., and H. Reuter. 1977. Reconstruction of the action potential of ventricular myocardial fibers. *J. Physiol. (Lond.).* 268:177–210.

Boersma, L., J. Brugada, C. Kirchhof, and M. Allessie. 1994. Mapping of reset of anatomic and functional reentry in anisotropic rabbit ventricular myocardium. *Circulation.* 89:852–862.

Buchanan, J. W., and L. S. Gettes. 1990. Ionic environment and propagation. *In* Cardiac Electrophysiology from Cell to Bedside. D. Zipes and J. Jalife, editors. W. B. Saunders Company, Philadelphia. 149–156.

Cha, Y. M., U. Birgersdotter-Green, P. L. Wolf, B. A. Peters, and P. S. Chef. 1994. The mechanism of termination of reentrant activity in ventricular fibrillation. *Circ. Res.* 74:495–506.

Colatski, T. J. 1992. Potassium channels blockers: synthetic agents and their antiarrhythmic potential. *In* Potassium Channels Modulator. A. H. Weston and T. C. Hamilton, editors. Blackwell Scientific Publications, London. 304–340.

Courtemanche, M. 1996. Complex spiral wave dynamics in a spatially distributed ionic model of cardiac electrical activity. *Chaos.* 6:579–600.

Courtemanche, M., and A. Winfree. 1991. Re-entrant rotating waves in the Beeler-Reuter based model of two-dimensional cardiac electrical activity. *Int. J. Bifurcation Chaos.* 1:2431–2444.

Daut, J. 1982. The passive electrical properties of guinea-pig ventricular muscle as examined with voltage clamp technique. *J. Physiol. (Lond.).* 330:221–242.

Davidenko, J. M., R. Salomonsz, A. M. Pertsov, W. T. Baxter, and J. Jalife. 1995. Effects of pacing reentrant activity. Theoretical and experimental study. *Circ. Res.* 77:1166–1179.

Davidenko, J. M., P. Kent, and J. Jalife. 1991a. Spiral waves in normal isolated ventricular muscle. *Physica. D.* 49:182–197.

Davidenko, J. M., A. M. Pertsov, R. Salomonsz, W. Baxter, and J. Jalife. 1991b. Stationary and drifting spiral waves of excitation in isolated cardiac muscle. *Nature.* 355:349–351.

Davidenko, J. M., P. Kent, D. R. Chialvo, D. C. Michaels, and J. Jalife. 1990. Sustained vortex-like waves in normal isolated ventricular muscle. *Proc. Natl. Acad. Sci. USA.* 87:8785–8789.

Delgado, C., B. Steinhaus, M. Delmar, D. R. Chialvo, and J. Jalife. 1990. Directional differences in excitability and margin of safety for propagation in sheep ventricular muscle. *Circ. Res.* 67:97–110.

Delmar, M. D., J. Ibarra, J. Davidenko, P. Lorente, and J. Jalife. 1991. Dynamic of the background outward current of single guinea pig ventricular myocytes: ionic mechanisms of hysteresis in cardiac cells. *Circ. Res.* 69:1316–1326.

Delmar, M., D. C. Michaels, T. Johnson, and J. Jalife. 1987. Effects of increasing intercellular resistance on transverse and longitudinal propagation in sheep epicardial muscle. *Circ. Res.* 60:780–785.

Ebihara, L., and E. A. Johnson. 1980. Fast sodium current kinetic in cardiac muscle: a quantitative description. *Biophys. J.* 32:779–790.

Efimov, I. R., V. I. Krinsky, and J. Jalife. 1995. Dynamics of rotating vortices in the Beeler-Reuter model of cardiac tissue. *Chaos Solitons Fractals.* 5:513–526.

Elharrar, V., and B. Surawicz. 1983. Cycle length effect on restitution of action potential duration in dog cardiac fibers. *Am. J. Physiol.* 244 (*Heart Circ. Physiol.* 13):H782–H792.

Fast, V. G., B. J. Darrow, J. E. Saffitz, and A. G. Kleber. 1996. Anisotropic activation spread in heart cell monolayers assessed by high-resolution optical mapping. *Circ. Res.* 79:115–127.

Fast, V. G., and A. G. Kleber. 1994. Anisotropic conduction in monolayers of neonatal rat heart cells cultured on collagen substrate. *Circ. Res.* 75:591–595.

Fast, V. G., and A. G. Kleber. 1993. Microscopic conduction in cultured strands of neonatal rat heart cells measured with voltage-sensitive dyes. *Circ. Res.* 73:914–925.

Fujii, S., R. K. Ayer, and R. Dehaan. 1988. Development of the fast sodium current in early embryonic chick heart cells. *J. Membr. Biol.* 101: 209–223.

Gerish, G. 1965. Standienpezifische aggregationsmuster bei *Distyostelium discoideum. Wihelm Roux Arch. Entwick Org.* 156:127–144.

Gorelova, N. A., and J. Bures. 1983. Spiral waves of spreading depression in the isolated chicken retina. *Neurobiology.* 14:353–363.

Gray, R. A., J. Jalife, A. Panfilov, W. T. Baxter, C. Cabo, J. M. Davidenko, and A. M. Pertsov. 1995. Nonstationary vortexlike reentrant activity as a mechanism of polymorphic ventricular tachycardia in the isolated rabbit heart. *Circulation.* 91:2454–2469.

Hodgkin, A. L., and A. F. Huxley. 1952. A quantitative description of membrane current and its application to conduction and excitation in nerve. *J. Physiol. (Lond.).* 117:500–544.

Hondeghem, L. M. 1994. Computer aided development of antiarrhythmic agents with class III_a properties. *J. Cardiovasc.* 5:711–721.

Hume, J. 1985. Ionic basis of the different action potential configurations of single guinea-pig atrial and ventricular myocytes. *J. Physiol. (Lond.).* 368:525–544.

Ibarra, J., G. E. Morley, and M. Delmar. 1991. Dynamics of the inward rectifier k+ current during the action potential of guinea pig ventricular myocytes. *Biophys. J.* 60:1534–1539.

Kleber, A. G., and C. B. Riegger. 1987. Electrical constants of arterially perfused rabbit papillary muscle. *J. Physiol. (Lond.).* 385:307–324.

Kodama, I., R. Suzuki, K. Murayama, and J. Toyama. 1995. Electrophysiological effects of SD-3212, a new antiarrhythmic agent with vasodilator action, on guinea-pig ventricular cells. *Br. J. Pharmacol.* 114: 503–509.

Kreyszig, E. 1972. Advanced Engineering Mathematics. John Wiley and Sons, New York.

Krinsky, V. I. 1978. Mathematical models of cardiac arrhythmias (spiral waves). *Pharmacol. Ther. B.* 3:539–555.

Krinsky, V. I., and I. R. Efimov. 1992. Vortices with linear cores in mathematical models of excitable media. *Physica A.* A88:55–60.

Lancaster, P., and K. Salkauskas. 1990. Curve and Surface Fitting: An Introduction, 3rd Ed. Academic Press, San Diego.

Lechleiter, J., S. Girard, E. Peralta, and D. Clapham. 1991. Spiral calcium wave propagation and annihilation in *Xenopus laevis* oocytes. *Science.* 252:123–126.

Leon, L. J., F. A. Roberge, and A. Vinet. 1994. Simulation of two-dimensional anisotropic cardiac reentry: effects of the wavelength on the reentry characteristics. *Ann. Biomed. Eng.* 22:568–591.

Liu, Y., W. Zeng, M. D. Delmar, and J. Jalife. 1993. Ionic mechanisms of electrotonic inhibition and concealed conduction in rabbit atrioventricular nodal myocytes. *Circulation.* 88:1634–1646.

Luo, C. H., and Y. Rudy. 1991. A model of ventricular cardiac action potential depolarization, repolarization and their interaction. *Circ. Res.* 68:1501–1526.

Luo, C. H., and Y. Rudy. 1994. A dynamic model of the cardiac ventricular action potential. I. Simulations of ionic currents and concentration changes. *Circ. Res.* 76:1071–1096.

Matsuura, H., T. Ehara, and Y. Imoto. 1987. An analysis of the delayed outward current in single ventricular cells of the guinea-pig. *Pflugers Arch.* 410:596–603.

Mikhailov, A. S., and V. S. Zykov. 1991. Kinematical theory of spiral waves in excitable media: comparison with numerical simulations. *Phys. D.* 52:379–397.

Muruyama, K., I. Kodama, T. Anno, R. Suzuki, and J. Toyama. 1995. Electrophysiological effects of Ro 22-9194, a new antiarrhythmic agent, on guinea-pig ventricular cells. *Br. J. Pharmacol.* 114:19–26.

Noble, D. 1990. Oxsoft Heart Program Manual. Oxsoft, Oxford.

Nordin, C. 1993. Computer model of membrane current and intracellular Ca^{2+} flux in the isolated guinea pig ventricular muscle. *Am. J. Physiol.* 265:H2117–H2136.

Pertsov, A. M., J. M. Davidenko, R. Salomonsz, W. T. Baxter, and J. Jalife. 1993. Spiral waves of excitation underlie reentrant activity in isolated cardiac muscle. *Circ. Res.* 72:631–650.

Pertsov, A. M., E. A. Ermakova, and A. V. Panfilov. 1984. Rotating spiral waves in modified FitzHugh-Nagumo model. *Physica D.* 14:117–124.

Reuter, H., and H. Scholz. 1977. A study of the ion selectivity and the kinetic properties of the calcium dependent slow inward current in mammalian cardiac muscle. *J. Physiol. (Lond.).* 264:17–47.

Robinson, R. B., and P. A. Boyden. 1987. Electrical restitution process in dispersed canine cardiac Purkinje and ventricular cells. *Am. J. Physiol.* 253(*Heart Circ. Physiol.*):H1018–1025.

Roth, B. J. 1997. Non-sustained reentry following successive stimulation of cardiac tissue through a unipolar electrode. *J. Cardiovasc. Electr.* 8:768–778.

Starmer, C. F., D. N. Romashko, R. S. Reddy, Y. I. Zilberter, J. Starobin, A. O. Grant, and V. I. Krinsky. 1995. Proarrhythmic response to potassium channel blockade. Numerical studies of polymorphic tachyarrhythmias. *Circulation.* 92:595–605.

Starobin, J. M., Y. I. Zilberter, E. M. Rusnak, and C. F. Starmer. 1996. Wavelet formation in excitable cardiac tissue: the role of wavefront-obstacle interactions in initiating high-frequency fibrillatory-like arrhythmias. *Biophys. J.* 70:581–594.

Weidman, S. 1970. Electrical constants of trabecular muscle from mammalian heart. *J. Physiol. (Lond.).* 210:1041–1054.

Winfree, A. T. 1972. Spiral waves of chemical activity. *Science.* 175: 634–636.

Winfree, A. T. 1986. When Time Breaks Down. Princeton University Press, Princeton, NJ.

Winfree, A. T. 1991. Varieties of spiral wave behavior: an experimentalist's approach to the theory of excitable media. *Chaos.* 1:303–334.

Zhou, X., P. Guse, P. Wolf, D. L. Rollins, W. M. Smith, and R. E. Ideker. 1992. Existence of both fast and slow channel activity during the early stages of ventricular fibrillation. *Circ. Res.* 70:773–786.